

An Image Segment-based Classification for Chest X-Ray Image

Phongsathorn Kittiworapanya

60070055@kmitl.ac.th

Faculty of Information Technology

King Mongkut's Institute of Technology Ladkrabang
Bangkok, Thailand

Kitsuchart Pasupa

kitsuchart@it.kmitl.ac.th

Faculty of Information Technology

King Mongkut's Institute of Technology Ladkrabang
Bangkok, Thailand

ABSTRACT

In late 2019, the first case of COVID-19 was confirmed in Wuhan, China. The number of cases has been rapidly growing since then. Molecular and antigen testing methods are very accurate for the diagnosis of COVID-19. However, with sudden increases of infected cases, laboratory-based molecular test and COVID-19 test kits are in short supply. Because the virus affects an infected patient's lung, interpreting images obtained from Computed Tomography Scanners and Chest X-ray Radiography (CXR) machines can be an alternative for diagnosis. However CXR interpretation requires experts and the number of experts is limited. Therefore, automatic detection of COVID-19 from CXR images is required. We describe a system for automatic detection of COVID-19 from CXR images. It first segmented images to select only the lung. The segmented part was then fed into a multiclass classification module, which worked well with samples obtained from various sources, which had different aspect ratios, contrast and viewpoints. The system also handled the unbalanced dataset—only a small fraction of images showed COVID-19. Our system achieved 92% of F_1 -score and 88.1% Marco F_1 -score on the 3rd Deep Learning and AI Summer/Winter School Hackathon Phase 3—Multi-class COVID-19 Chest X-ray challenge public leaderboard.

CCS CONCEPTS

• **Computing methodologies** → **Computer vision**; • **Applied computing** → **Life and medical sciences**.

KEYWORDS

COVID-19, Coronavirus, Computer Vision, Neural Networks, Imbalanced Data

ACM Reference Format:

Phongsathorn Kittiworapanya and Kitsuchart Pasupa. 2020. An Image Segment-based Classification for Chest X-Ray Image. In *CSBio '20: Proceedings of the Eleventh International Conference on Computational Systems-Biology and Bioinformatics (CSBio2020)*, November 19–21, 2020, Bangkok, Thailand. ACM, New York, NY, USA, 7 pages. <https://doi.org/10.1145/3429210.3429227>

Permission to make digital or hard copies of all or part of this work for personal or classroom use is granted without fee provided that copies are not made or distributed for profit or commercial advantage and that copies bear this notice and the full citation on the first page. Copyrights for components of this work owned by others than ACM must be honored. Abstracting with credit is permitted. To copy otherwise, or republish, to post on servers or to redistribute to lists, requires prior specific permission and/or a fee. Request permissions from permissions@acm.org.

CSBio2020, November 19–21, 2020, Bangkok, Thailand

© 2020 Association for Computing Machinery.

ACM ISBN 978-1-4503-8823-8/20/11...\$15.00

<https://doi.org/10.1145/3429210.3429227>

1 INTRODUCTION

Severe Acute Respiratory Syndrome-Related (SARS-CoV-2), also known as COVID-19, is an acute respiratory diseases [16]. In late 2019, it has started as an outbreak in Wuhan, China. The number of cases rapidly increased in China and other countries and the World Health Organization (WHO) declared the COVID-19 outbreak as a pandemic on 11 March 2020 [23], because the number of infections outside China had rapidly grown to over a million cases. This affected the global public health system and created millions of demand for a cure.

Most patients infected by COVID-19 had a mild to moderate fever, sore throat and cough. However, some cases were asymptomatic, passed temperature checks and some where even unaware that they had caught the virus [22]. Moreover, the virus also caused abnormal lung condition. Currently, there are many kinds of COVID-19 tests, that can be split into two groups—diagnostic and antibody tests.

Diagnostic active infection tests include molecular and antigen testing. It is necessary to collect a specimen by swabbing nasal or throat areas. Then the specimen is sent to a laboratory to extract genetic material of the virus. Alternatively, a doctor can use a COVID-19 test kit. Both tests are very accurate. The dramatic increase in infections has lead to a shortage laboratory-based molecular-assay tests and COVID-19 test kits.

COVID-19 affects the infected patient's lung. thus diagnosing COVID-19 from lung images, obtained from a Computed Tomography (CT) Scanner or a Chest X-ray Radiography (CXR) machine, can play a significant role [25]. Ai *et al.* in China started to diagnose COVID-19 from CT images [1] and showed that it achieved a sensitivity of 88%, while Reverse-Transcription Polymerase Chain Reaction (RT-PCR) from swabs obtained only 59%. Although a CT scanner can obtain more details of the object than a CXR machine does, it is more expensive and requires more time to scan. Most clinical sites only have a CXR machine because it is cheaper, a CXR image can diagnose the damage to lungs from COVID-19. Further, using a portable CXR scanner can avoid the relocation of patients and reduce the risk of cross-infection [21].

Experts are needed to interpret CXR images and the number of experts is limited. Therefore, the automatic detection of COVID-19 from X-ray images is needed. Computer vision and machine learning techniques are becoming effective to tackle medical problems, *e.g.* red blood cells morphology classification [18], malarial parasite counting and classification [11] and MRI image analysis [15]. Here, we describe an automatic approach for diagnosing COVID-19 and other lung diseases from CXR images, using computer vision and deep learning techniques. This work can assist health workforces as well as reducing human error.

This paper is organized: Section 2 describes related works on COVID-19 CXR image classification. Section 3 explains the methods used, including datasets, algorithms, experiment framework, and evaluation metrics. We compare and discuss the experimental results in Section 4. Section 5 concludes.

2 RELATED WORKS

Many researchers have used computer vision and deep learning techniques for detection of COVID-19 and other diseases, *e.g.* pneumonia, from CT and CXR images.

Zhang *et al.* [26] introduced confidence-aware anomaly detection for CXR images. The technique included feature extraction from a backbone network, built on ResNet18. These features were employed for classification with a contrastive loss to optimize the detection between anomaly and non-anomaly cases and a confidence prediction network for error correction. Ozturk *et al.* [17] described ‘DarkCovidNet’, inspired by the DarkNet architecture to provide accurate diagnostics for both binary classification (COVID-19 or not) and multiclass classification (COVID-19 or not or Pneumonia) tasks. Wang *et al.* [14] introduced COVID-Net, which used a projection-expansion-projection design pattern, which provided enhanced representational capacity, while still maintains computational effectively.

Several works focused on the lung image segmentation task. Candemir *et al.* [3] used a content-based image retrieval approach to identify a set of CXR images that are most similar to the patient X-ray, using partial Radon transforms, combined with a Bhattacharyya similarity measure. Then, it used a graph cuts discrete optimization approach to determining lung boundaries. Jaeger *et al.* [9] used a graph-cut segmentation method for lung segmentation, then features were extracted from the segmented parts before using a Support Vector Machine algorithm for automatic Tuberculosis screening task. Win *et al.* [24] used hybrid learning approach from deep-activated features from CNN model and hand crafted features for classifying tuberculosis from CXR image.

None of these works supported COVID-19 with multiclass classification task with various types of CXR image input for, *e.g.* different viewpoints and various image resolutions, due to various CXR image sources or different CXR scanners. This problem can degrade the performance of the model. Thus, our system handled this situation by removing irrelevant parts from the image, *e.g.* stomach, liver, from the CXR image and kept the only lungs. The idea is to determine the area of the lungs by image segmentation techniques based on deep learning techniques, *i.e.* U-Net [20], Feature Pyramid Network (FPN) [12], DeepLab [5]. U-Net was solely designed for medical image segmentation and based on convolutional neural networks. FPN used a pyramid representation for object detection while DeepLab consists of atrous convolution, fully connected Conditional Random Fields and deep convolutional network.

3 METHODS

This section describes the methods used in this work. It includes descriptions of a dataset, our new system that consists of data preprocessing, image segmentation and classification modules and experiment settings. Evaluation metrics are explained at the end of the section.

Table 1: DLAI3 Dataset Distribution

Classes	Number of Images			Class Prior
	Train	Validate	Totals	
COVID-19	272	91	363	6.60%
Thorax-Diseases	2,794	931	3,736	25.61%
Clear	1,056	352	1,408	67.78%
Total	4,122	1,374	5,507	100%

3.1 Dataset

In this work, we focused on the Deep Learning and AI Summer/Winter School (DLAI) Hackathon Phase 3—Multiclass COVID-19 Chest X-ray Challenge dataset [4]: it was collected from various sources, *i.e.* a pneumonia dataset from a study on children, thorax CXR images from U.S. National Library of Medicine (NIH) and unverified clear images from NIH. The dataset consists of three classes that are ‘‘COVID-19’’, ‘‘Thorax-Diseases’’, and ‘‘Clear’’. Note that the ‘‘Clear’’ label in this dataset does not necessarily imply ‘‘Normal’’; it implies clear of thorax diseases and may contains instances of other disease patterns or uncertain findings. Examples of each class are illustrated in Figure 1). The CXR images have a different aspect ratios, contrasts and viewpoints. Some CXR images show only half of the patient’s lung and some images cover from neck to stomach. These problems require data preprocessing before feeding into the network. The dataset contains 5,507 images—divided into 363 COVID-19 3,736 Thorax Diseases and 1,408 ‘‘Clear’’.

3.2 Our CXR COVID-19 Diagnosis System

Our system has three main steps—preprocessing, segmentation and classification steps—see Figure 2. First, the CXR image passes through the preprocessing module. The lung segmentation module takes a preprocessed CXR image and returns a binary mask of the lung area. Then, the image is cropped based on a bounding box for the lung segment. The cropped image is then fed to a classifier for the three classes.

3.2.1 Data Preprocessing. The original RGB X-ray images were converted to monochrome images, with floating point pixels, to match the requirements of CNN network inputs. We randomly split the dataset into training and test sets with an 80–20 split. The distributions of the training and test sets are shown in Table 1. In addition, augmentation increased the number of training set and enabled the model to be more robust and able to understand uncommon CXR images— which have only half of the lung. We randomly cropped an image on the area of the lung, To augment the data set, a random selection of one or more the following operations— random cropping on lung area, horizontal and vertical flipping, 90 degree rotation and histogram equalization— were applied to the original images. Although the data set was augmented, the proportion of each class remained the same.

3.2.2 Lung Segmentation. Deep learning models for semantic segmentation were used for lung image segmentation. Common three state-of-the-art models are selected, including U-Net with Xception encoder, Feature Pyramid Networks (FPN) with Xception encoder

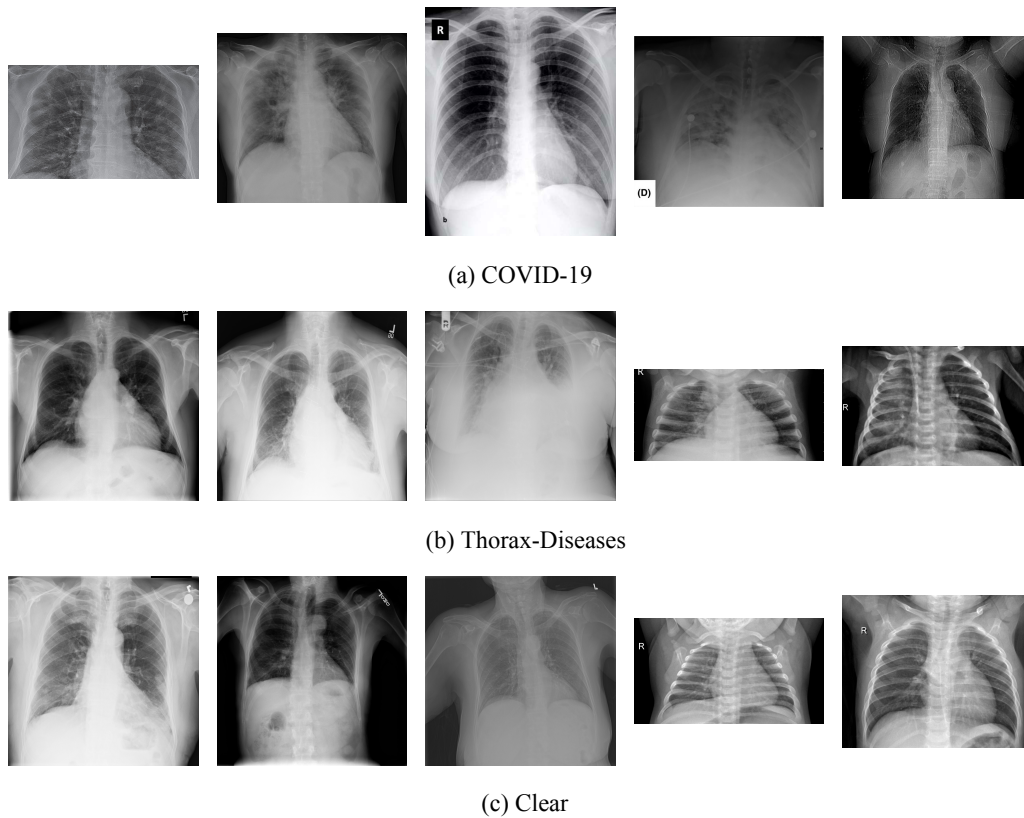


Figure 1: Examples of DLAI Hackathon Phase 3—Multiclass COVID-19 Chest X-ray Challenge dataset

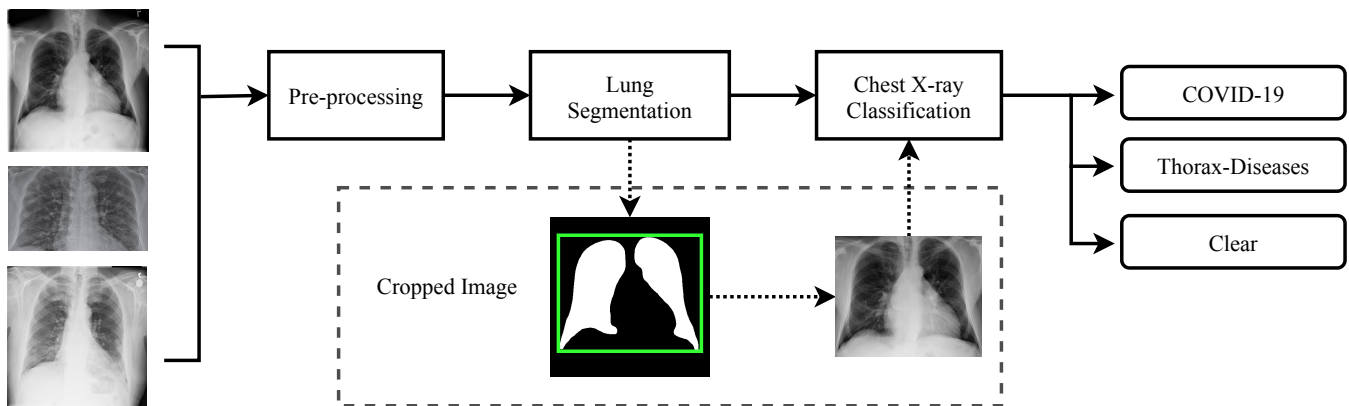


Figure 2: Our CXR COVID-19 Diagnosis Framework

and DeepLab with ResNet50 encoder. All three models were pre-trained with the ImageNet dataset.

A transfer learning technique was used by fine-tuning the pre-trained model by a lung segmentation dataset. The pre-trained models were fine-tuned with MC-Shenzhen Postero-anterior Chest Radiographs (MC-Shenzhen)—a publicly available dataset from U.S. National Library of Medicine [8]. Each sample has a CXR image and a manual lung segmentation in a binary mask. This dataset came

from a collaboration between the Department of Health and Human Services, Montgomery County, Maryland, USA and Shenzhen No.3 People’s Hospital, Guangdong Medical College, Shenzhen, China. There are 706 pairs of images and segmentations in this dataset. We randomly divided the dataset into two sets of 528 training and 176 test data. The dataset was augmented in the pre-processing step.

3.2.3 CXR Classification. In this step, a CNN model categorized CXR images into three classes. Three commonly used state-of-the-art CNN based models were selected, ResNet [7] with 18 and 50 layers, referred to as ResNet18 and Resnet50, respectively, and Xception [6]. ResNet is a residual learning model that used skip connections to solve the gradient vanishing problem, when the depth of CNN layer increases. ResNet settings are shown in Table 2. Xception is a CNN model, that is based on depthwise separable convolution layers. The mapping of cross-channel and spatial correlations in the feature maps of CNN can be entirely decoupled and were linearly stacked with residual connections. This enhanced the overall accuracy.

The DLAI3 dataset is an unbalanced dataset—only 6.6% of the samples are COVID-19—the minority class. To solve this problem, there are two approaches—data sampling and algorithmic adjusting. Data sampling manipulates each class to have an equal distribution. For example, by up-sampling that augments the samples in the minority class to match the majority class. On the other hand, a down-sampling reduces the majority class. Algorithmic adjusting modifies the algorithm to consider the minority class, i.e., modify loss function. A common loss function for an unbalanced dataset is called “Focal loss”. It enables the model to focus on the minority class samples. In this work, we used focal loss in the model.

Focal loss is developed from a Cross entropy loss function. Cross entropy for a multi-class task is computed as

$$CE(y, \hat{y}) = - \sum_{c=1}^M y_c \log(\hat{y}_c) \quad (1)$$

where y_c is probability of ground truth of class c , \hat{y}_c is a predicted probability and M is a number of considered classes. The aim of focal loss is to put more weight on hard samples and can be represented as

$$FL(y, \hat{y}) = -\alpha_c (1 - \hat{y}_c)^\gamma \log(\hat{y}_c) \quad (2)$$

where α_c is the weight of balanced cross-entropy of the c -th class, $\alpha \in [0, 1]$, and γ is a modulating factor of cross-entropy loss.

3.3 Experiment Settings

All three lung image segmentation models were fine-tuned from the publicly available model—U-Net, FPN, DeepLab by MC-Shenzhen dataset. All images were resized with locked aspect ratios and padded to square 512×512 pixel images. CE was used as the loss function. An Adam optimizer [10] with loss plateau decay—a dynamic reduce learning rate when the loss was not improving—was used. Batch size was set to 4, and the maximum number of epochs was 100. In fine-tuning, the first three residual blocks of ResNet50 encoder and the first two convolutional layers of Xception encoder were frozen, while the other layers were adjusted.

In the classification task, the input images were also resized, while the aspect ratio is kept. Images were padded into a square 224×224 pixel images for ResNet and 299×299 pixels for Xception. In this module, CE and FL functions were used. An Adam optimizer with a learning rate of 0.001 and weight decay of 0.0001 was used. The maximum number of the epochs was 300.

There are two parameters in FL— γ and α_c . We simply set $\gamma = 2$, because it was shown to be the best by Pasupa *et al.* [13, 19]. α_c was set according to the prior probability of c of DLAI3 dataset, that

Table 2: ResNet Architecture Settings

Layer	Output size	18-layers	50-layers
conv1	112×112	7×7, 64, stride 2	
		3×3 max pool, stride 2	
conv2_x	56×56	$\begin{bmatrix} 3 \times 3, 64 \\ 3 \times 3, 64 \end{bmatrix} \times 2$	$\begin{bmatrix} 1 \times 1, 64 \\ 3 \times 3, 64 \\ 1 \times 1, 256 \end{bmatrix} \times 3$
conv3_x	28×28	$\begin{bmatrix} 3 \times 3, 128 \\ 3 \times 3, 128 \end{bmatrix} \times 2$	$\begin{bmatrix} 1 \times 1, 128 \\ 3 \times 3, 128 \\ 1 \times 1, 512 \end{bmatrix} \times 4$
conv4_x	14×14	$\begin{bmatrix} 3 \times 3, 256 \\ 3 \times 3, 256 \end{bmatrix} \times 2$	$\begin{bmatrix} 1 \times 1, 256 \\ 3 \times 3, 256 \\ 1 \times 1, 1024 \end{bmatrix} \times 6$
conv5_x	7×7	$\begin{bmatrix} 3 \times 3, 512 \\ 3 \times 3, 512 \end{bmatrix} \times 2$	$\begin{bmatrix} 1 \times 1, 512 \\ 3 \times 3, 512 \\ 1 \times 1, 2048 \end{bmatrix} \times 3$
	1×1	average pool, 1000-D fc, softmax	

is $1 - P_c$. Hence, α_c was 0.9340 for COVID-19 0.3221 for Thorax diseases and 0.7438 for the No-finding classes.

3.4 Evaluation Metrics

We used several metrics to measure the quality of the models for segmentation and classification.

3.4.1 Segmentation Task. A ground truth mask (y) and a predicted mask (\hat{y}) were compared. Here we used two metrics:

- Dice’s Coefficient (D) measures the overlap between ground truth segmentation and predicted segmentation masks

$$D = \frac{2 \cdot |y \cap \hat{y}|}{|y| + |\hat{y}|} \quad (3)$$

- Intersection-Over-Union (IoU) is a metric that measures how well a predicted mask is similar to the ground truth mask and ranged from 0–1. IoU is the area of overlap between the predicted and the ground truth segmentation divided by the area of union between the predicted segmentation and the ground truth:

$$IoU = \frac{|y \cap \hat{y}|}{|y \cup \hat{y}|} \quad (4)$$

3.4.2 Classification Task. We used common metrics including accuracy, precision, recall, F_1 -score and Matthews Correlation Coefficient (MCC). The F_1 -score can be calculated:

$$F_1\text{-score} = \frac{2 \cdot \text{precision} \cdot \text{recall}}{\text{precision} + \text{recall}} \quad (5)$$

MCC is a metric that measures the quality of classification which produces a high score when the prediction obtained good results in True Positive (TP), True Negative (TN), False Positive (FP) and False Negative (FN). The MCC ranges between $[-1, +1]$, $+1$ represents a perfect classification, 0 represents the worst, and -1 is inverse prediction. MCC can be calculated as,

$$MCC = \frac{TP \times TN - FP \times FN}{\sqrt{(TP + FP)(TP + FN)(TN + FP)(TN + FN)}} \quad (6)$$

4 RESULTS AND DISCUSSION

We started with a focus on lung image segmentation models. The three segmentation models—U-Net, FCN with Xception encoder, and DeepLab with ResNet50 encoder—were fine-tuned and evaluated on the MC-Shenzhen dataset. Table 3 reports segmentation performance with Dice’s coefficient and IoU. FPN can achieved the best IoU and Dice’s coefficient followed by DeepLab and U-Net. Therefore, we selected FPN as our core model for lung image segmentation.

Table 3: Performance of segmentation algorithms on the MC-Shenzhen dataset

Model	IoU	Dice’s Coefficient
U-Net	0.970	0.618
FPN	0.972	0.621
DeepLab	0.970	0.619

After that, we cropped the lung segment in each image to remove parts irrelevant for COVID-19 diagnosis. Then, the cropped images were used for training the classification module. We further evaluated with conventional loss, CE, and the imbalance loss, FL, with all models. Results are in Table 4. We also compared our system with and without the segmentation module.

Table 4 shows that the Xception network yielded the best results in all cases, except the Xception network, without the lung image segmentation module in conjunction with the FL case, followed by ResNet18. Moreover, employing FL in the model improved the F_1 -score and MCC score in most cases. Only the F_1 -score and MCC score of ResNet50, without the lung segmentation module and with the FL case, was slightly worse than without the FL ($\sim 1\%$). Although, the F_1 -score and MCC score for Xception with CE and FL without segmentation modules were the same, recall of the model with FL was slightly better. Also, using segmentation module did not seem to improve the overall performance. The segmentation module did not include the whole area of the lung in some cases. Therefore, removing parts from the images removed detail for diagnosis of the disease. Figure 3 shows examples in the validation set where the segmentation module failed to include all the lung area. Thus, the best model was the Xception network, in conjunction with FL and without lung segmentation.

We further investigated our system on a test set from the DLAI3 dataset, that contains 1,130 images without the label, part of “DLAI3 Hackathon Phase 3—Multi-class COVID-19 Chest X-ray challenge” [2]. To obtain the performance of the model, we submitted the predicted output to the challenge. The final score will be shown on the public

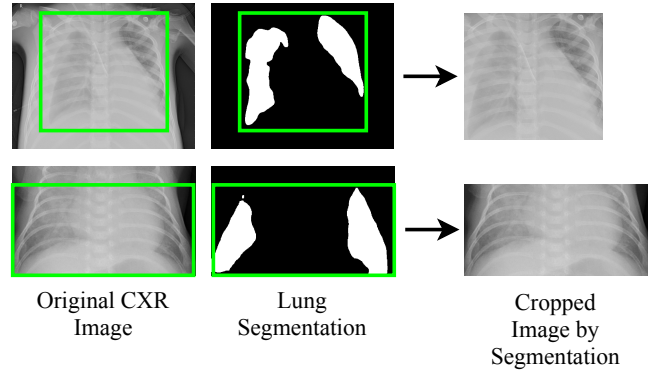


Figure 3: Examples of images where segmentation module failed to detect the whole lung

leaderboard. The challenge used the Marco F_1 -score to determine the best algorithm. The scores of our approach, obtained from the challenge, are shown in Table 5. The scores listed in the public leaderboard was computed from 30% of the test set. The final score will be announced when the challenge is closed. Table 5 shows that Xception with CE and lung segmentation modules yielded the best F_1 -score at 88.1%. In the overall picture, the segmentation module improves performance by 8.1% on CE and 2.7% on FL, on average across all the models.

This performance was not comparable with that on the validation set. We attribute this to either (a) the segmentation model can perform well on the test set, or (b) the test set consisted of images from various sources. Examples of these images are shown in Figure 4. Unfortunately, the FL could only improve the performance of ResNet18 and ResNet50 without the segmentation module.



Figure 4: Examples of images in test set

Since lung segmentation and FL improved the overall performance, we computed confusion matrices for the Xception model with lung segmentation in conjunction with CE and FL on the validation set as shown in Figure 5). They show that, with FL, the Xception model achieved 14% improvement on COVID-19 cases. This shows that FL enabled the model to focus on the minority class.

Table 4: Classification Experiment Results

	Method	CE					FL				
		Accuracy	Precision	Recall	F1	MCC	Accuracy	Precision	Recall	F1	MCC
Without Lung Image Segmentation	ResNet18	98%	98%	95%	96%	0.95	98%	97%	96%	97%	0.96
	ResNet50	97%	97%	95%	96%	0.94	97%	96%	95%	95%	0.93
	Xception	98%	98%	96%	97%	0.96	98%	98%	97%	97%	0.96
	Average	97.7%	97.7%	95.3%	96.3%	0.95	97.7%	97.3%	96%	96.3%	0.95
With Lung Image Segmentation	ResNet18	94%	90%	89%	89%	0.87	94%	91%	91%	91%	0.87
	ResNet50	93%	87%	90%	88%	0.85	93%	87%	90%	89%	0.85
	Xception	95%	94%	90%	92%	0.89	94%	91%	93%	92%	0.88
	Average	94%	90.3%	89.7%	89.7%	0.87	93.7%	89.7%	91.3%	90.7%	0.87

Table 5: Model performance on the test set provided on DLAI3 Hackathon Phase 3 Scores. Macro F_1 was used as a evaluation matric and reported in DLAI3 Challenge Public Leaderboard. Noted that these numbers are only the performance of 30% of the test set.

	Method	CE	FL
Without Lung Segmentation	ResNet18	77.0%	79.4%
	ResNet50	69.3%	72.8%
	Xception	83.8%	81.6%
	Average	76.7%	77.9%
With Lung Segmentation	ResNet18	82.6%	80.6%
	ResNet50	83.8%	77.2%
	Xception	88.1%	83.9%
	Average	84.8%	80.6%

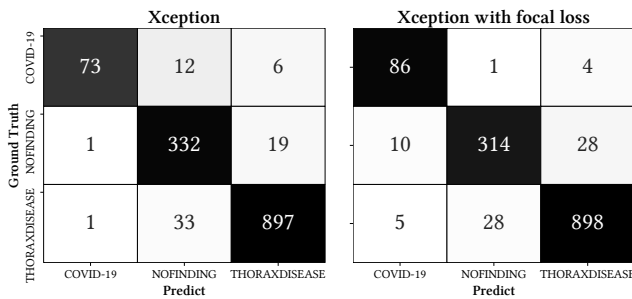


Figure 5: Confusion matrix of Xception with Lung segmentation module and with CE (left) and FL (right).

5 CONCLUSION

In rapidly growth of COVID-19 cases. Other way to diagnose COVID-19 by using CXR image become more useful. We designed a system to diagnose COVID-19, Thorax diseases and others that affect an infected patient’s lung from chest X-ray images from various sources. With a limited number of COVID-19 images collected from different CXR scanners with various viewpoints, we segmented out irrelevant parts, e.g. stomach, and liver, to improve COVID-19 classification. The available data set was unbalanced, due to the small number of COVID-19 classes compared to other

lung diseases. So we used a modified loss function, ‘focal loss’, to make the CNN model focus on the minority class, so as to better handle the unbalanced classes— in the CXR images.

In future work, we aim to improve the performance of lung image segmentation. This can improve the overall performance because the output of the model will be fed into the classification model.

REFERENCES

- [1] Tao Ai, Zhenlu Yang, Hongyan Hou, Chenao Zhan, Chong Chen, Wenzhi Lv, Qian Tao, Ziyong Sun, and Liming Xia. 2020. Correlation of chest CT and RT-PCR testing in coronavirus disease 2019 (COVID-19) in China: a report of 1014 cases. *Radiology* 296, 2 (2020), E32–E40. <https://doi.org/10.1148/radiol.2020200642>
- [2] APNNS/IEEE. 2020. DLAI3 Hackathon Phase 3—Multi-class COVID-19 Chest X-ray challenge. <https://www.kaggle.com/c/dlai3-phase3> [Online; accessed 31 Aug. 2020].
- [3] S. Candemir, S. Jaeger, K. Palaniappan, J. P. Musco, R. K. Singh, Z. Xue, A. Karargyris, S. Antani, G. Thoma, and C. J. McDonald. 2014. Lung Segmentation in Chest Radiographs Using Anatomical Atlases With Nonrigid Registration. *IEEE Transactions on Medical Imaging* 33, 2 (Feb 2014), 577–590. <https://doi.org/10.1109/TMI.2013.2290491>
- [4] Jonathan H. Chan. 2020. DLAI3 Hackathon Phase3 COVID-19 CXR Challenge. <https://doi.org/10.34740/KAGGLE/DSV/1347344>
- [5] Liang-Chieh Chen, George Papandreou, Iasonas Kokkinos, Kevin Murphy, and Alan L Yuille. 2018. Deeplab: Semantic image segmentation with deep convolutional nets, atrous convolution, and fully connected crfs. *IEEE transactions on pattern analysis and machine intelligence* 40, 4 (April 2018), 834–848. <https://doi.org/10.1109/TPAMI.2017.2699184>
- [6] F. Chollet. 2017. Xception: Deep Learning with Depthwise Separable Convolutions. In *Proceedings of the IEEE Conference on Computer Vision and Pattern Recognition (CVPR 2017)*. IEEE, Honolulu, HI, 1800–1807. <https://doi.org/10.1109/CVPR.2017.195>
- [7] K. He, X. Zhang, S. Ren, and J. Sun. 2016. Deep Residual Learning for Image Recognition. In *Proceedings of the IEEE Conference on Computer Vision and Pattern Recognition (CVPR 2016)*. IEEE, Las Vegas, NV, USA, 770–778. <https://doi.org/10.1109/CVPR.2016.90>
- [8] Stefan Jaeger, Sema Candemir, Sameer Antani, Yi-Xiang J. Wang, Pu-Xuan Lu, and George Thoma. 2014. Two public chest X-ray datasets for computer-aided screening of pulmonary diseases. *Quantitative Imaging in Medicine and Surgery* 4, 6 (2014), 475–477. <https://doi.org/10.3978/j.issn.2223-4292.2014.11.20>
- [9] S. Jaeger, A. Karargyris, S. Candemir, L. Folio, J. Siegelman, F. Callaghan, Z. Xue, K. Palaniappan, R. K. Singh, S. Antani, G. Thoma, Y. Wang, P. Lu, and C. J. McDonald. 2014. Automatic Tuberculosis Screening Using Chest Radiographs. *IEEE Transactions on Medical Imaging* 33, 2 (Feb 2014), 233–245. <https://doi.org/10.1109/TMI.2013.2284099>
- [10] Diederik P. Kingma and Jimmy Ba. 2015. Adam: A Method for Stochastic Optimization. In *Proceedings of the 3rd International Conference on Learning Representations, (ICLR 2015)*. San Diego, CA, USA. <http://arxiv.org/abs/1412.6980>
- [11] W. Kudisthalert, K. Pasupa, and S. Tongshima. 2020. Counting and Classification of Malarial Parasite From Giemsa-Stained Thin Film Images. *IEEE Access* 8 (2020), 78663–78682. <https://doi.org/10.1109/ACCESS.2020.2990497>
- [12] T. Lin, P. Dollár, R. Girshick, K. He, B. Hariharan, and S. Belongie. 2017. Feature Pyramid Networks for Object Detection. In *Proceedings of the 2017 IEEE Conference on Computer Vision and Pattern Recognition (CVPR)*. IEEE, Honolulu, HI, 936–944.

- <https://doi.org/10.1109/CVPR.2017.106>
- [13] T. Lin, P. Goyal, R. Girshick, K. He, and P. Dollar. 2017. Focal Loss for Dense Object Detection. In *Proceedings of the 2017 IEEE International Conference on Computer Vision (ICCV)*. IEEE Computer Society, Los Alamitos, CA, USA, 2999–3007. <https://doi.org/10.1109/ICCV.2017.324>
- [14] Zhong Qiu Lin Linda Wang and Alexander Wong. 2020. COVID-Net: A Tailored Deep Convolutional Neural Network Design for Detection of COVID-19 Cases from Chest Radiography Images. arXiv:2003.09871 [cs.CV]
- [15] Alexander Selvikvåg Lundervold and Arvid Lundervold. 2019. An overview of deep learning in medical imaging focusing on MRI. *Zeitschrift für Medizinische Physik* 29, 2 (2019), 102–127. <https://doi.org/10.1016/j.zemedi.2018.11.002>
- [16] Coronaviridae Study Group of the International et al. 2020. The species Severe acute respiratory syndrome-related coronavirus: classifying 2019-nCoV and naming it SARS-CoV-2. *Nature Microbiology* 5, 4 (2020), 536. <https://doi.org/10.1038/s41564-020-0695-z>
- [17] Tulin Ozturk, Muhammed Talo, Eylul Azra Yildirim, Ulas Baran Baloglu, Ozal Yildirim, and U. Rajendra Acharya. 2020. Automated detection of COVID-19 cases using deep neural networks with X-ray images. *Computers in Biology and Medicine* 121 (2020), 103792. <https://doi.org/10.1016/j.combiomed.2020.103792>
- [18] Kitsuchart Pasupa, Suchat Tungjitnob, and Supawit Vatathanavaro. 2020. Semi-supervised Learning With Generative Adversarial Networks for Canine Red Blood Cells Morphology Classification. *Multimedia Tools and Applications* (2020). <https://doi.org/10.1007/s11042-020-08767-z>
- [19] Kitsuchart Pasupa, Supawit Vatathanavaro, and Suchat Tungjitnob. 2020. Convolutional Neural Networks based Focal Loss for Class Imbalance Problem: A Case Study of Canine Red Blood Cells Morphology Classification. *Journal of Ambient Intelligence and Humanized Computing* (2020). <https://doi.org/10.1007/s12652-020-01773-x>
- [20] Olaf Ronneberger, Philipp Fischer, and Thomas Brox. 2015. U-net: Convolutional networks for biomedical image segmentation. In *Proceedings of the International Conference on Medical Image Computing and Computer-Assisted Intervention (MICCAI 2015)*. Springer, Munich, Germany, 234–241. https://doi.org/10.1007/978-3-319-24574-4_28
- [21] Geoffrey D. Rubin, Christopher J. Ryerson, Linda B. Haramati, Nicola Sverzellati, Jeffrey P. Kanne, Suhail Raoof, Neil W. Schluger, Annalisa Volpi, Jae-Joon Yim, Ian B.K. Martin, Deverick J. Anderson, Christina Kong, Talissa Altes, Andrew Bush, Sujal R. Desai, Jonathan Goldin, Jin Mo Goo, Marc Humbert, Yoshikazu Inoue, Hans-Ulrich Kauczor, Fengming Luo, Peter J. Mazzone, Mathias Prokop, Martine Remy-Jardin, Luca Richeldi, Cornelia M. Schaefer-Prokop, Noriyuki Tomiyama, Athol U. Wells, and Ann N. Leung. 2020. The Role of Chest Imaging in Patient Management During the COVID-19 Pandemic: A Multinational Consensus Statement From the Fleischner Society. *Chest* 158, 1 (2020), 106–116. <https://doi.org/10.1016/j.chest.2020.04.003>
- [22] Tanu Singhal. 2020. A Review of Coronavirus Disease-2019 (COVID-19). *The Indian Journal of Pediatrics* 87 (03 2020). <https://doi.org/10.1007/s12098-020-03263-6>
- [23] Catrin Sohrabi, Zaid Alsafi, Niamh O'Neill, Mehdi Khan, Ahmed Kerwan, Ahmed Al-Jabir, Christos Iosifidis, and Riaz Agha. 2020. World Health Organization declares global emergency: A review of the 2019 novel coronavirus (COVID-19). *International Journal of Surgery* 76 (2020), 71–76. <https://doi.org/10.1016/j.ijisu.2020.02.034>
- [24] Khin Yadanar Win, Noppadol Maneerat, Kazuhiko Hamamoto, and Syna Sreng. 2020. Hybrid Learning of Hand-Crafted and Deep-Activated Features Using Particle Swarm Optimization and Optimized Support Vector Machine for Tuberculosis Screening. *Applied Sciences* 10, 17 (Aug 2020), 5749. <https://doi.org/10.3390/app10175749>
- [25] Wenjing Yang, Arlene Sirajuddin, Xiaochun Zhang, Guanshu Liu, Zhongzhao Teng, Shihua Zhao, and Minjie Lu. 2020. The role of imaging in 2019 novel coronavirus pneumonia (COVID-19). *European Radiology* 30, 9 (April 2020), 4874–4882. <https://doi.org/10.1007/s00330-020-06827-4>
- [26] Jianpeng Zhang, Yutong Xie, Zhibin Liao, Guansong Pang, Johan Verjans, Wenxin Li, Zongji Sun, Jian He, Yi Li, Chunhua Shen, and Yong Xia. 2020. Viral Pneumonia Screening on Chest X-ray Images Using Confidence-Aware Anomaly Detection. arXiv:2003.12338 [eess.IV]